Exp # 81
Submitted to Phys. Rev. C
FERMILAB-PUB-79-092-E

RECEIVED
FEB 12 1979
DIRECTORS OFFICE
FERMILAB

# Nuclear Reactions of Silver with 25.2 GeV $^{12}C$ Ions and 300 GeV Protons

N. T. Porile, G. D. Cole, and C. R. Rudy
Department of Chemistry, Purdue University,
W. Lafayette, IN 47907

Cross sections for the production of approximately 100 radionuclides in the interaction of silver with 25.2 GeV $^{12}C$ ions and 300 GeV protons have been determined. The results have been parametrized in terms of a 10-parameter equation which accurately reproduces the measured isobaric- and mass-yield curves. The cross sections of products in the A=40-106 mass range are consistent with the factorization hypothesis. At lower mass numbers, the yields of products formed in reactions induced by $^{12}C$ ions are enhanced by over a factor-of-two relative to the ratio of total reaction cross sections. The results are compared with Monte Carlo cascade-evaporation calculations and with the abrasion-ablation model.

NUCLEAR REACTIONS Ag($^{12}C$, spallation) and Ag(p, spallation) $E_{^{12}C}$ = 25.2 GeV, $E_p$ = 300 GeV. Production cross sections for ∿ 100 radionuclides; deduced charge dispersions and mass-yield curves. Comparison with cascade-evaporation and abrasion-ablation calculations.

## I. Introduction

The interaction of relativistic heavy ions with complex nuclei has been the subject of many investigations in recent years. These have revealed an unexpected variety of processes ranging from the gentle removal of a single nucleon from the target nucleus to the violent breakup of the composite system into a spectacularly large number of nucleons and particles. It has been found convenient to divide the interactions into three broad categories on the basis of the rapidities of the products. Projectile fragmentation involves the formation of products with rapidities centered about that of the projectile. This process, which is a prominent feature of reactions induced by relativistic heavy ions, has been widely investigated.[1-3] Target fragmentation leads to products having rapidities close to that of the target and is equivalent to the process commonly known as spallation in high-energy proton reactions. A number of studies of this process have been reported.[4-8] Both of these types of reactions appear to be the result of peripheral collisions. The third category involves the formation of products having intermediate rapidities. These products, which appear to be concentrated in the light-fragment mass region, are thought to result from central collisions in which regions of highly excited nuclear matter are produced.[9-12]

The present work is concerned with one particular experimental approach to the study of relativistic heavy ion reactions, namely, the determination of the distribution in Z and A of the residual nuclei resulting from the interaction. The dependence on A of the total isobaric cross section, $\sigma_A$, is commonly referred to as the mass-yield curve while

the variation with Z of the cross sections for the production of nuclides of a given mass number is variously called the charge dispersion or the isobaric-yield distribution. The results of such experiments provide information on target fragmentation and central collisions but are completely insensitive to projectile fragmentation for targets of moderate thickness. Measurements of this type have long constituted one of the important approaches to the study of reactions of high-energy protons with complex nuclei. In addition to the many qualitative features of the interaction that may be derived from a phenomenological analysis of the data, comparisons with Monte Carlo cascade-evaporation calculations have permitted a more detailed examination of reaction mechanisms. The recent availability of cascade calculations for heavy ions[13-15] makes similar comparisons possible for these reactions. Since the calculations are based on the assumption that the reaction is propagated by collisions between individual quasi-free nucleons, the comparison serves to indicate the extent to which these reactions may be explained without invoking collective effects not included in the model.

A useful feature of charge-dispersion and mass-yield determinations in relativistic heavy ion reactions is the possibility of comparison with similar results obtained for reactions of high-energy protons with the same target. Such a comparison permits a separation of those features that are common to both types of reactions from those that are different, and presumably not as well understood. More specifically, the comparison permits an examination of the validity of the factorization hypotheses,[16] which states that the cross sections for products of target fragmentation should depend on the identity of the projectile only via a factorable

total cross section term. Although it is not completely clear whether such a comparison should be made at the same total energy or the same energy per nucleon of the projectiles in question, the limiting fragmentation hypothesis[16] suggests that at sufficiently high bombarding energies fragmentation cross sections should reach their asymptotic values. In this regime the two comparisons should thus yield identical results.

Most of the previous investigations of this type have been performed on copper targets. In a series of articles, Cumming and collaborators have reported the mass-yield curve for the interaction of copper with 3.9 GeV $^{14}N$ ions,[4] 25 GeV $^{12}C$ ions,[5] and 80 GeV $^{40}Ar$ ions.[8] Comparative measurements were also performed for 3.9 and 28 GeV protons. These experiments confirmed the general validity of limiting fragmentation and factorization at bombarding energies of 2-4 GeV and above. The shape of the mass-yield curve was thus found to be independent of bombarding energy in this high-energy regime. Furthermore, the ratios of cross sections for the formation of products in the $A \geq 20$ mass region in reactions induced by these projectiles were found to be independent of product mass number and, in those cases where absolute cross sections had been determined, consistent with calculated[17,18] ratios of total reaction cross sections. The only deviation occurred for the very lightest products, having $A < 10$, where a yield enhancement was observed for heavy ions relative to protons. Unfortunately, this conclusion was based on results for only one, or at most two products. In addition to the extensive results reported for copper, the only other mass-yield measurements reported to date have been some preliminary results for uranium,[6] gold,[7] and lead.[7]

The present study involves a determination of the charge dispersion and mass-yield curve for the interaction of silver with 25.2 GeV $^{12}C$ ions and a comparison with similar data obtained for 300 GeV protons. The greater mass range of products that can be formed from silver should permit a clearer delineation between target fragmentation and central collisions than was possible for copper. On the other hand, the fission cross section of silver is sufficiently small[19] to permit comparison of the results with cascade-evaporation calculations[15] which do not take this process into account. Although there have been several studies of the interaction of silver with high-energy protons[20-22] we chose to repeat these measurements in order to obtain the greater accuracy in the comparison that can be achieved by the use of the same experimental techniques and data analysis codes. These earlier proton studies showed that the cross sections had become independent of energy perhaps by 12 GeV, and certainly by 29 GeV. A comparison between cross sections obtained for 25 GeV $^{12}C$ ions and 300 GeV protons thus is equivalent to one between the former and 25 GeV protons. Our choice of 300 GeV protons was simply dictated by their availability. In addition to a phenomenological analysis of the data we present a comparison with Monte Carlo calculations[15] as well as with a simple geometric model of relativistic heavy ion reactions, the abrasion-ablation model,[23] which has had some measure of success in reproducing the main features of charge dispersions and mass-yield curves.[24] A preliminary account of the present research has been previously published.[25]

## II. Experimental

The irradiations with 2.1 A GeV $^{12}C$ ions were performed in an external beam line at the Lawrence Berkeley Laboratory Bevalac. The targets consisted of either 250 μm or 75 μm thick silver foils of high purity (99.999%) surrounded by 25 μm thick silver guard foils. These foils were preceded on the upstream side by a 75 μm aluminum foil surrounded by 25 μm Al guard foils. The purpose of the Al foil was to serve as a relative beam intensity monitor on the basis of the induced $^{24}Na$ activity.

The target stack was mounted on the upstream side of an Ar-$CO_2$ filled ion chamber used to determine the beam intensity. The chamber had been calibrated by measurement of the charge collected when a known number of 5 GeV protons traversed it.[26] The number of protons was determined on the basis of the number of $^{11}C$ nuclei produced in a carbon foil and the known[27] cross section of the $^{12}C(p,pn)$ reaction. The charge obtained in this fashion agreed to within 5% with a value based on the known energy loss of 5 GeV protons in Ar and $CO_2$ and the partial pressures of these gases in the chamber.[28] The calibration for protons was applied to $^{12}C$ ions on the assumption that the latter were fully stripped and so deposited 36 (i.e. $Z^2$) times more energy than protons of the same incident energy. The response of the chamber was found to be linear over a wide range of proton intensities.[26] The agreement between the cross section of the $^{27}Al(^{12}C,X)^{24}Na$ reaction based on the ion chamber readings and an independent estimate[8] indicates that the chamber was performing satisfactorily during the irradiations. In particular, the effect on the calculated beam intensities of secondary charged particles passing through the chamber could be neglected, a result that is reasonable in view of the

moderate target thicknesses used in this work. The charge collected in the chamber was recorded on a strip chart recorder which was calibrated before each series of bombardments by feeding in an accurately known charge from a standard cell. In addition to providing a value of the fluence, the record of the time dependence of the beam intensity was used to correct the cross sections of short-lived products for variations in beam intensity.

Seven separate irradiations were performed ranging in duration from one to eight hours. The beam intensity varied between $5 \times 10^8$ and $10^{10}$ ions per minute. The beam spot was usually close to circular in shape with a diameter of 1-2 cm. The target stack, which had dimensions of $5 \times 5$ $cm^2$, was positioned so that the beam passed through the center.

Following the irradiations the silver foils were assayed with calibrated Ge(Li) $\gamma$-ray spectrometers. Measurements were performed at both LBL and Purdue commencing in some cases between 8 and 13 minutes after the end of bombardment and continuing in others for as long as 1.5 years. The various detectors used in this work were intercalibrated with National Bureau of Standards (NBS) mixed radionuclide $\gamma$-ray emission-rate standards. The spectra were analyzed with the code SAMPO[29] and the decay curves of individual $\gamma$-rays were fit with the code CLSQ.[30] The particular version of CLSQ used in this work permitted the separate determination of parent and daughter activities in cases where both members of a genetically related pair of nuclides contributed to an observed peak. Nuclidic assignments were made on the basis of $\gamma$-ray energies and half-lives. Confirmatory evidence for the assignments was obtained from the relative intensities of the other known $\gamma$-rays, if any, emitted by the presumed nuclides.

The γ-ray abundances and half-lives were taken from a recent compilation,[31] updated in some instances with more recent information.[32] Of the 380 distinct γ-rays that were observed, nuclidic assignments were made for 280, and cross sections of 99 nuclides were determined on the basis of 230 γ-rays. A more complete description of this procedure has been published.[21]

A number of corrections were applied to the γ-ray disintegration rates. Because of the relatively thick targets used in this work, the disintegration rates of low-energy γ-rays had to be corrected for attenuation in the target. This correction amounted to at most 13% and was usually much smaller. The cross sectional area of the $^{12}C$ beam led to a spatial distribution of radionuclides that was considerably more extended than that of the NBS calibration standard. A correction for the difference in geometry was applied on the basis of equations derived by Jaffey.[33] The effect ranged from 2 to 4% depending on the particular detector and sample-to-detector distance. Due to the relatively low $^{12}C$ ion beam intensity the samples had to be assayed in relatively high geometry in order to obtain adequate counting rates. As a result, it was necessary to apply a correction for reduction in photopeak efficiency due to summing between the detected and coincident γ-rays. A code based on the formulation by McCallum and Coote[34] was written for this purpose. In addition to the detailed decay scheme information for each nuclide,[32] the input data included the relevant geometric parameters as well as low-geometry detector efficiencies. The corrections for nuclides emitting several coincident γ-rays typically amounted to 10-30%, depending on the particular sample-detector configuration.

The 300 GeV proton irradiations were performed in an external beam line at Fermilab. Every effort was made to match as closely as possible the conditions of the $^{12}C$ experiments. The target stacks were thus identical to those described above. The samples were assayed with the same or comparable Ge(Li) spectrometers at similar sample-detector distances. The activities of short-lived nuclides were determined at Fermilab and counting commenced about 15 minutes after the end of bombardment. Longer-lived nuclides were assayed at Purdue for periods ranging up to one year after bombardment. The various detectors were intercalibrated with NBS standards. The spectra were analyzed with the same codes and the same types of corrections were applied to the data. Four separate proton irradiations were performed.

The proton experiments did differ in three significant respects from the $^{12}C$ experiments. First, the irradiations had a duration of less than two minutes because the proton beam intensity was at least a factor of $10^3$ higher than the $^{12}C$ intensity. As a result, there was no need to apply corrections for beam intensity fluctuations for even the shortest-lived nuclides. Second, the proton beam was more narrowly focused than the $^{12}C$ beam and the extended source correction could be neglected. Third, the cross sections were determined relative to that of the $^{27}Al(p,3pn)$ reaction, whose value was taken as 8.6 mb.[35] The $^{24}Na$ activity in the Al monitor was determined by $\gamma$-ray spectrometry in the same manner as the activities of the products from silver.

## III. Results

### A. Secondary Effects

Since projectile fragmentation constitutes a potentially significant source of secondary particles, it is necessary to determine the magnitude of secondary processes in relativistic heavy ion reactions. This can be done by an examination of the dependence of the measured cross sections on target thickness. Fig. 1 shows the ratios obtained for the "thick" (250 μm) and "thin" (75 μm) targets in $^{12}C$ bombardments as a function of product mass number. A statistical analysis of the ratios showed that they are independent of mass number for products with $A \leq 90$. The weighted average value of the cross-section ratios is 1.05±0.03,indicating the occurrence of a small secondary effect even for products far from the target. The observed enhancement amounts to approximately 2.5% per 100 $mg/cm^2$ of silver. The cross-section ratios for products with $A \geq 90$ are more consistent with a linear dependence on A than with a constant value and a linear least-squares fit was performed. The maximum ratio, obtained for A = 106, is 1.45±0.14 indicating the occurrence of a substantial secondary effect for products close to the target. The measured cross sections were corrected for the contribution from secondary reactions by performing a linear extrapolation to zero target thickness, a procedure that is appropriate when the range of the secondary particles exceeds the target thickness. The uncertainties in the measured cross sections were increased by incorporating errors based on the standard deviations in the ratios.

The behavior of the cross section ratios obtained from the proton irradiations is more complex since it reflects the combined effect of

secondary contributions to the reactions of silver and to the monitor reaction. The cross sections of products with $A \leq 90$ thus had to be increased by 2.8% per 100 mg/cm$^2$ Ag indicating that the secondary contribution to the monitor reaction was larger than that to the Ag products. The cross sections of products in the A = 90-100 mass region were found to be independent of target thickness showing that the secondary contribution to the monitor was equal to that to silver products in this mass region. For $A > 100$ the cross sections had to be decreased by 5.3% per 100 mg/cm$^2$ Ag as the secondary contribution to products with mass numbers close to that of the target was now larger than that to the monitor reaction. The measured cross sections were corrected for these effects in the same way as the $^{12}$C values. The above comparison shows that, for products close to the target, the contribution of secondary processes is substantially larger for reactions induced by $^{12}$C ions than for those induced by protons.

B. Cross sections

The corrected cross sections are listed in Table I, each entry being the weighted average of as many as seven separate determinations. The tabulated uncertainties are the larger of the standard deviation and the estimated uncertainty of the individual determinations. The latter are based on the propagation of the errors obtained in the SAMPO and CLSQ fits and in addition include a 5% uncertainty in detector efficiencies. The individual cross-section determinations of nuclides emitting more than one assayed γ-ray are actually weighted averages of the separate γ-ray cross sections. We have arbitrarily folded in a 5% uncertainty in the

cross sections of nuclides having only a single assayed γ-ray. It is estimated that the $^{12}C$ cross sections are subject to a systematic error of 10-20% resulting from the ion chamber calibration but this error has not been incorporated in the tabulated values. The proton data have a similar uncertainty of ∿ 8% arising from that in the monitor reaction cross section.

The $^{7}Be$ cross sections had to be corrected for recoil loss from the target. We estimate a 5% loss from the 300 μm thick target and guard foil stack on the basis of the differential cross sections for the emission of $^{7}Be$ fragments in the interaction of silver with 5 GeV protons.[36] The correction is larger for the $^{12}C$-induced reaction because the fragment spectra are harder than those obtained in proton reactions. Although the spectra of interest have not been reported for reactions of silver with heavy ions, such data are available for uranium.[12] Assuming that the ratio of the fraction of energetic ($T \geq 100$ MeV) $^{7}Be$ fragments emitted in heavy ion and proton reactions of silver is the same as it is for uranium[12,37] we estimate a 20% recoil loss of $^{7}Be$ in heavy ion induced reactions. The tabulated cross sections have been corrected for this effect and a 50% uncertainty in the magnitude of the correction has been incorporated in the errors. The recoil loss effect for heavier products is negligibly small.

While some of the cross sections represent independent yields (I), the majority are cumulative. These are identified as either C+ or C- depending, respectively, on whether they represent the integrated isobaric cross section of more neutron-deficient or more neutron-excessive precursors. In some instances the measured cross sections include only

a partial contribution from the decay of isobaric progenitors and these cases are designated PC. In a few instances insufficient information about the decay scheme of the parent nuclide is available to permit an assessment of the nature of the yield.

One type of reaction that, in principle, can occur in reactions induced by $^{12}C$ ions but not in those induced by protons is the formation of trans-target products by the transfer of a nucleon or cluster from the projectile to the target. A search for the formation of such products was made in the studies of the interaction of copper with relativistic heavy ions.[4,5,8] Although some products were detected, they appeared to be primarily due to reactions induced by secondary particles. We investigated the possible production of such nuclides in the interaction of silver with $^{12}C$ ions and did indeed detect $^{110}Ag^{m}$ and $^{111}In$ at a level of several mb. However, the dependence of the cross sections on target thickness indicates that these products are primarily, if not entirely, due to secondary reactions. This is not surprising in view of the large momentum mismatch between projectile and target nucleons.

While our measurements provide the first cross sections of the reactions of Ag with $^{12}C$ ions, results for high-energy protons in the regime where limiting fragmentation appears to be valid have been obtained previously.[20,22] Katcoff, Fickel and Wyttenbach[20] have measured the distribution of radionuclides from the interaction of silver with 29 GeV protons. In this work most of the radioactivity measurements were performed with NaI detectors on radiochemically separated samples. Of the 42 cross sections common to the two studies, 25 are in very good agreement, i.e. within 15%, and only 7 differ by more than 50%. A cursory examination of

these data indicates that the large discrepancies are at least in part due to differences in the assumed decay schemes. If these cases are excluded, the average difference between the two sets of cross sections is 9%.

English, Yu, and Porile[22] measured the cross sections of radionuclides produced in 300 GeV proton bombardment of silver in a very similar experiment to the present one. The main difference between the two studies lies in the techniques of spectral analysis. In the earlier work a much less sophisticated code was thus used to obtain the $\gamma$-ray intensities. These two studies contain 59 common cross sections of which 38 agree to within 15% and only 5 differ by more than 50%. Once again, these large differences are at least in part due to differences in assumed branching ratios. Excluding these cases, the average difference between the two sets of cross sections is 11%.

C. Cross section of the $^{27}Al(^{12}C,X)^{24}Na$ monitor reaction

Although our experiment was not designed to measure the cross section of a beam monitor reaction such as that involving the formation of $^{24}Na$ from $^{27}Al$, the inclusion of Al foils in most of the target stacks made such a measurement possible. The data were treated in the same manner as the silver cross sections. The results obtained for Al foils incorporated in the 75 μm and 250 μm thick silver target stacks were separately averaged. A secondary effect of approximately 4% per 100 mg/cm$^2$ of silver was noted. The weighted average cross section corrected for this effect was found to be 19.4±3.9 mb, where a 15% uncertainty in the ion chamber calibration has been folded into the quoted error. Cumming et al.[8] have recently estimated the value of this cross section on the

basis of the measured value of the $^{27}Al(^{40}Ar,X)^{24}Na$ cross section and the application of the factorization hypothesis to reactions induced in Al by $^{40}Ar$ and $^{12}C$ ions. Their derived value of 18±3 mb is in agreement with our experimental value.

D. Parametrization of nuclidic cross sections

Although the number of separate cross sections measured in this work, approximately 100 for both $^{12}C$ ions and protons, is substantial, the data add up to only a fraction of the total reaction cross section. In order to obtain the mass-yield curve, estimates of unmeasured cross sections must be made. Rudstam[38] has proposed a semi-empirical equation for the cross sections of spallation products. His 6-parameter equation assumes that the mass-yield curve decreases exponentially with decreasing product mass number and that, at a given mass number, the isobaric yield distribution is Gaussian. We were unable to obtain an adequate fit to our data with this equation. This is primarily due to the fact that at medium- and low-mass numbers the contribution of processes other than spallation becomes important and the mass-yield curve, in fact, appears to go through a minimum. Cumming et al.[4] have fit their copper data with a modified form of the Rudstam equation. These workers represented this equation as a polynomial in mass number, A, and used a non-linear least squares fitting routine to determine the number of terms that yielded the best fit to the data. In addition, the isobaric yield distribution was allowed to be asymmetric by the inclusion of an exponential tail on the neutron-rich side of the maximum.

We have adopted the approach of Cumming et al.[4] and fit our data

with a number of different polynomials of varying order. The best overall fit was obtained with the following 10-parameter equation:

$$\sigma(Z,A) = \exp[\alpha_1+\alpha_2 A+\alpha_3 A^2+\alpha_4 A^3 + (\alpha_5+\alpha_6 A+\alpha_7 A^2)|Z_p-Z|^{\alpha_8}] \qquad (1)$$

The first four parameters, $\alpha_1$-$\alpha_4$, determine the shape of the mass-yield curve. Cumming et al.[4] were able to fit their copper data for products in the A=37-57 mass range using only the first two of these parameters. The more complex shape of the mass yield over the much broader mass range of present interest requires two additional terms in the series. The parameters $\alpha_5$ - $\alpha_7$ determine the width of the isobaric yield distribution. The inclusion of the two A-dependent terms is an indication of the fact that the width is mass dependent. The parameter $\alpha_8$ determines the shape of the isobaric yield distribution at a given mass number. A Gaussian distribution corresponds to $\alpha_8 = 2$. A smaller value of $\alpha_8$ leads to a broader distribution in the region of the wings and gives a somewhat better fit to the data than the asymmetric curve used by Cumming et al.[4] The isobaric yield distribution is symmetric about the most probable charge, $Z_p$. The most satisfactory form of the relation between $Z_p$ and product mass number was found to be

$$Z_p = \alpha_9 A + \alpha_{10} A^2 \qquad (2)$$

which is identical to the relation used by Rudstam.[38]

The $^{12}C$ and proton data in the A = 20-100 mass range were separately fit with Eq. (1) by iterative use of a non-linear least-squares code. In the first iteration, Eq. (1) was fit to cumulative and independent yields

alike. The cumulative cross sections were then corrected by means of the calculated progenitor cross sections and the corrected data were refit. This procedure converged after three or four iterations. We did not follow this approach for products with A > 100. In this mass range the isobaric yield distribution ceases to be symmetric as a result of the effective cutoff imposed by the low probability of producing nuclides with atomic number higher than that of the target. Furthermore, a comparison of the cross sections of nuclides that should be equally displaced from $Z_p$, e.g. $^{105}$Rh and $^{103}$Ru, indicates that the mass-yield curve varies more rapidly close to the target than at somewhat lower mass numbers. A graphical charge dispersion analysis was performed in order to determine the mass-yield curve in this region.

The results of the parametrization are summarized in Table 2, in which the values of $\alpha_1 - \alpha_{10}$ obtained for both the $^{12}$C and proton experiments are tabulated. The quality of the parametrization may be determined from a comparison of the data with the calculated isobaric-yield distributions and mass-yield curves, respectively. In order to compare the independent yields derived from the measured cross sections with the isobaric-yield distribution it is convenient to divide both experimental and calculated cross sections by the calculated value of $\sigma_A$ in order to obtain fractional isobaric yields, designated $F_{exp}$ and $F_{calc}$, respectively. If the isobaric-yield distribution were independent of mass number, all the values of $F_{exp}$ would lie on a single curve. The inclusion of the $\alpha_6$ and $\alpha_7$ terms in the cross-section parametrization indicates that this is not the case. In order to permit a comparison of all the data with a single calculated curve, and

thereby avoid the necessity of dividing the mass range into a number of narrow regions, it is convenient to scale the values of $F_{exp}$ to a common mass number by defining a corrected value of this quantity, $F_{cor}$, as

$$F_{cor}((Z_p-Z), A) = F_{exp}((Z_p-Z), A) \left[ \frac{F_{calc}((Z_p-Z), A=70)}{F_{calc}((Z_p-Z), A)} \right] \quad (3)$$

In this expression the experimental fractional yield of nuclide (Z,A) is adjusted by the ratio of the calculated fractional yields at A=70 and the A value in question, where the F values are evaluated at the same distance from the most probable charge at the respective mass numbers. This procedure preserves the agreement, or lack thereof, between the various experimental and calculated fractional yields and collapses all the yields onto a single mass number, arbitrarily chosen as A=70.

Figure 2 shows a comparison of the $F_{cor}$ values with the calculated fractional isobaric yield distribution evaluated at A=70 by means of the parameters listed in Table II. The proton data include some of the published results for 29 GeV protons,[20] particularly those for products lying far from the maximum and thus able to better define the shape of the curve. The calculated curves give a reasonably good fit to the data although a number of isolated discrepancies may be noted, particularly for the $^{12}C$ distribution. This is not surprising in view of the fact that the much lower $^{12}C$ ion beam intensity resulted in greater statistical uncertainties in these data. The different symbols assigned to the $F_{cor}$ values identify the mass region of the products. A close examination of the figure shows no systematic mass-dependent discrepancies.

The values of $\sigma_A$ obtained from the data are compared with the mass-

yield curves based on the parametrization in Fig. 3. The points are the experimental cross sections, corrected for the unmeasured portion of the isobaric yield by means of Eq. (1). The different symbols indicate the fraction of the isobaric cross section that was experimentally determined. The error bars incorporate a 20% uncertainty in the unmeasured contributions to the isobaric cross sections. While some discrepancies may be noted, on the whole the curves fit the data rather well.

## IV. Discussion

### A. Comparison of the charge-dispersion and mass-yield curves in reactions induced in silver by $^{12}C$ ions and protons

The similarities and differences between the isobaric and mass-yield distributions obtained in $^{12}C$ and proton reactions are implicit in a comparison of the $\alpha_1 - \alpha_{10}$ parameters. Of all these parameters, only $\alpha_8$ uniquely determines some property of the distributions. As mentioned above, this parameter fixes the shape of the isobaric yield distribution at a given mass number. The value of $\alpha_8$ is nearly the same for both projectiles and is substantially smaller than 2, the value yielding a Gaussian distribution. The isobaric yield distributions are thus somewhat more sharply peaked and, at the same time, significantly broader in the region of low fractional yields than a Gaussian distribution.

Two useful measures of the changes in the charge dispersion with mass number are the variation of $Z_p$ and of the full-width at half-maximum (FWHM) with A. These quantities are plotted in Fig. 4. (We actually plot $Z_p/A$ which, according to Eq. (2), is linear in A). It is seen that the most probable charge is virtually identical for both projectiles at

all mass numbers. Also included in this figure is the variation of $Z_A$, the most stable charge at mass number A. The peak in the isobaric yield distribution occurs on the neutron deficient side of stability down to about A=40, the displacement ranging from about 0.7 to 1.4 Z units. In the vicinity of this mass number the $Z_A$ and $Z_p$ curves cross and the yield distribution at lower mass numbers peaks on the neutron-rich side of stability.

The bottom panel in Fig. 4 shows the mass dependence of the widths. For both projectiles the widths increase with A, first slowly and then more rapidly, the increase being particularly pronounced at A > 80 for $^{12}C$. This increase in width is a reflection of the gradual broadening of the valley of stability with increasing A, which favors the distribution of the isobaric yield among a larger number of nuclides. Although the width of the $^{12}C$ distribution is substantially greater than that of the proton distribution at all mass numbers, the difference is not outside the uncertainties derived from those in the parameters. It thus appears that there is very little, if any, difference in the charge dispersions for reactions of $^{12}C$ ions and protons with silver.

Also shown in Fig. 4 are some of the values of $Z_p$ and the width derived by Katcoff, Fickel and Wyttenbach[20] from their study of the interaction of silver with 29 GeV protons. These workers performed a non-parametric analysis of the data and the quantities of interest are based on charge-dispersion curves hand-drawn through independent or near-independent yields of products lying in narrow mass intervals. The values of $Z_p$ are in excellent agreement with the present results but those of the full-width tend to be larger and show a less systematic trend with mass

number. This is probably just a reflection of the variability in the shape of the hand-drawn curves coupled with the sizeable uncertainties in the values of this parameter.

The mass-yield curves are compared in Fig. 3. Both curves display four common features. First, the cross sections decrease sharply with decreasing A in the vicinity of the target. Products in this mass region result from the most peripheral interactions, in which few nucleons are knocked out of the target and little energy transfer occurs. Next, the cross sections decrease exponentially over an interval of approximately 40 mass numbers down to A $\sim$ 60. This is the mass region where spallation is the dominant mechanism. In this region our parametrization predicts essentially the same dependence of $\sigma_A$ on A as the simpler Rudstam formula.[38] This mass region is followed by one of essentially constant yields extending downward to A=30-40. Differential range measurements performed on products from the interaction of silver with 2.9 GeV protons[39] indicate that the range of $^{43,44}$Sc is consistent with spallation, so that this process is expected to be of importance even in this rather light mass region. While the fission cross section of silver for 29 GeV $^{14}$N ions is only 8 mb,[19] and that for comparable energy protons is even smaller,[40] this mechanism will contribute to the production of nuclides lying at the lower end of the mass interval in question.[39] Finally, the mass-yield curves turn up at the lowest mass numbers, reflecting the contribution of fragment emission. The one striking difference between the two mass-yield curves in fact occurs in this mass region. It is thus apparent that the upturn in yields is considerably more pronounced in the $^{12}$C curve. We shall consider this difference in more detail in the

context of the cross-section ratios.

The proton mass-yield curve in Fig. 3 includes the most accurately determined total isobaric cross sections due to Katcoff, Fickel, and Wyttenbach.[20] Their points generally scatter about and follow the curve based on the present results. The only systematic difference occurs close to the target, where their yields show a much smaller mass dependence. The paucity of the data available in this region makes it difficult to draw any firm conclusions about the total isobaric yields.

The distribution in product yields from the interaction of $^{12}C$ ions with silver is displayed in somewhat different form in Fig. 5, which shows a contour plot of the cross sections in the Z-N plane. The various contours correspond to a factor-of-two difference in cross section. There are two widely separated 12 mb contours. The upper one commences at $A \sim 70$ and extends up to the vicinity of the target. A 25 mb contour occurs at the upper end of the mass range, beginning at $A \sim 102$. These contours lie on the neutron-deficient side of stability and the probability of forming products on the neutron-rich side of the $Z_A$ line is small. The other 12 mb contour first becomes apparent at $A \sim 34$ and extends downward from this mass number. The beginnings of a 25 mb contour are seen at $A \sim 21$. In contrast to the high-yield contours at the upper end of the mass range, the low A contours are centered on the neutron-rich side of $Z_A$. Nonetheless, the N/Z values about which the yields in this mass region are centered are substantially lower than the N/Z value of the target, and somewhat lower than the N/Z of the most probable products near the target. The difference in the location of the contours at low and high A is thus due to the change in the location of the $Z_A$ line in the

Z-N plane rather than to any intrinsic change in $Z_p$.

The ratios of the $^{12}C$ to the proton cross sections are displayed in Fig. 6. The points represent either the ratios of individual cross sections, or, in cases where more than one isobaric measurement was available, those of the measured isobaric yields. The curve is the ratio of the parametrized mass-yield curves. If the factorization hypothesis is obeyed, these ratios should be equal to that of the total reaction cross sections, $\sigma_R(^{12}C)/\sigma_R(P)$.

The horizontal lines in Fig. 6 represent two estimates of $\sigma_R(^{12}C)/\sigma_R(P)$. The top line is based on Karol's calculated value of $\sigma_R(^{12}C)$ for 2.1A GeV carbon ions[18] and the experimental value of $\sigma_R(P)$ determined by Ashmore et al.[41] for 24 GeV protons. The bottom line is obtained from our own parametrized values of $\sigma_A$, summed between A=30 and 106. The summation was stopped at A=30 on the assumption that lighter products had heavier partners and had thus already been counted. The 10% difference between these lines primarily reflects the uncertainty in both the calculated and experimental values of $\sigma_R(^{12}C)$. The experimental ratios scatter about a value of 1.9, and are thus consistent with the ratio of total reaction cross sections at all mass numbers down to approximately A=40. At lower mass numbers, the values of $\sigma_{^{12}C}/\sigma_P$ are seen to increase substantially above the ratio of the reaction cross sections and, below A $\sim$ 30, are enhanced relative to this ratio by over a factor-of-two. If the comparison had been made at the same energy per nucleon instead of at the same total energy of the projectiles, the enhancement would have been even greater. The cross sections for the production of these nuclides in reactions induced by protons thus increase by a factor-of-two between 3

and 29 GeV.[20] Enhanced yields of light fragments have previously been reported for reactions induced in copper by $^{12}C$ ions,[5] albeit only for products having $A < 10$. Similar enhancements have been reported for fragments with $Z \leq 15$ from the interaction of gold with 2.1A GeV $^{16}O$ ions[9] and for Z=2-5 fragments emitted in the interaction of uranium with various 2.1A GeV heavy ions.[12] The enhanced emission of light fragments thus appears to be a general feature of relativistic heavy ion reactions and is indicative of the importance of interactions in which high excitation energies are transferred to the struck nucleus.

B. Comparison with Monte Carlo cascade-evaporation calculations

In this section we compare our results with Monte Carlo cascade-evaporation calculations. Yariv and Fraenkel[15] have recently adapted the Vegas intranuclear cascade code[42,43] to reactions initiated by heavy ions. The Vegas code (ISOBAR version) incorporates the formation and subsequent scattering and decay of single $\Delta$ isobars in nucleon-nucleon collisions, and so is considered to be applicable up to a bombarding energy of $\sim$ 1 GeV. The heavy ion code ISABELLE[15] represents the incident $^{12}C$ ion as a nucleus having the same type of density distribution and nuclear potential as assumed in the Vegas code for the target nuclei. The separate nucleon-nucleon collisions of the twelve incident nucleons are followed simultaneously, thereby permitting the depletion of nucleons in the interaction region, an effect that is particularly important in heavy-ion reactions, to be incorporated in the calculation. Two different prescriptions for this depletion effect are available. In one option (infinite rearrangement time, $t_r = \infty$) a "hole" is punched in the nuclear density at the position in configuration space at which a nucleon was lifted out of the Fermi sea and remains stationary with respect to the center of the

nucleus during the rest of the cascade. The density elsewhere in the nucleus is not affected. In the other option (zero rearrangement time, $t_r$=0) the density of the whole nucleus is reduced after each collision. The actual situation presumably lies somewhere between these two limits. The results presented below were obtained with the first of these options but results of somewhat limited statistical significance were also obtained for the second option.

The ISABELLE code was run for 1A GeV $^{12}C$ ions incident on both $^{107}Ag$ and $^{109}Ag$. The deexcitation of the residual nuclei was accomplished by use of the evaporation code EVA, which is based on the DFF evaporation formalism.[44] The calculated results do not include evaporation residues from projectile fragmentation and, as mentioned before, neither do the experimental data. Although comparison is made with results obtained for 2.1A GeV $^{12}C$ ions, we do not expect this difference in energy to be significant. The results obtained by Cumming and collaborators for copper[4,5] thus show that the mass yield and charge dispersion are independent of energy in this regime.

The calculated mass-yield curve is compared with the experimental points in Fig. 7. In order to minimize statistical fluctuations, the calculated cross sections have been binned in $\Delta A$ = 5 intervals. It is seen that the calculation fits the data remarkably well. Excellent agreement is thus obtained both in the mass region closest to the target, where Monte Carlo cascade calculations have often had problems in fitting data, and in the A=60-100 mass region. Examining the situation at lower mass numbers, it can be seen that the calculation overestimates the yield of products in the A=45-60 region by some 20%, a difference that is out-

side the uncertainties in both experiment and calculation. On the other hand, satisfactory agreement is once again obtained at A=40-45. The formation of products removed as many as 70 mass numbers from the target by spallation requires the deposition of very high excitation energies in the struck nuclei. The calculation thus indicates that $^{12}C$ ions are effective in depositing such high energies. The calculation does not, of course, predict the upturn in the yield of the lightest products since the emission of such fragments lies outside the scope of the cascade-evaporation model. It is nonetheless worthy of note that the predicted spallation yields remain above the 5 mb level all the way down to A=25. The observed yield of these light fragments may thus contain a significant spallation contribution.

The calculated mass-yield curve obtained with the $t_r=0$ option is somewhat flatter than that displayed in Fig. 7. It thus predicts lower yields in the $A \geq 90$ mass region and higher yields for $A < 60$. In this respect it appears to be in poorer agreement with the data than the $t_r = \infty$ option.

The calculation is compared in further detail with the data in Fig. 8, which displays the isotopic yield distributions of various elements ranging from Sc to Pd. Data are presented for those elements for which at least four isotopic yields were measured. Cumulative experimental yields were corrected for the contribution of isobaric progenitors by means of Eq. (1). The calculated cross sections are depicted by the two sets of lines, which lie one standard deviation above and below the calculated value. The main impression obtained from this comparison is that while the calculation correctly predicts the location of the peak yields, the isotopic-yield distributions are much flatter than is observed experimentally. These conclusions are buttressed by a

parametrization of the calculated cross sections by means of Eqs. (1) and (2). This analysis shows that the charge dispersion is much broader than the experimental curve, although both curves are centered on essentially the same value of $Z_p$. For instance at A=70 the calculated full width is 2.54 Z units and the experimental value is 1.36 Z units, while the corresponding $Z_p$ are 32.0 and 32.1, respectively. It thus appears that the calculation severely overestimates the widths of the isobaric and isotopic yield distributions. Since the DFF evaporation calculation has had considerable success in reproducing isobaric yield ratios,[44,45] it appears likely that the cascade calculation must overestimate the width of the isobaric yield distribution of cascade residues.

Bondorf, Fai, and Nielsen[46] have recently considered the effect of isospin correlations in the nuclear ground state on the isobaric yield distribution obtained in relativistic heavy ion reactions. The isospin potential prevents the occurrence of large local differences in the neutron and proton densities and so leads to a narrower isobaric yield distribution of the products of the initial interaction than would be obtained in the absence of such correlations. While the deexcitation of the primary residues should smear this effect out to some extent, the resulting distribution of the final products should still be narrower. These authors thus estimate that in the interaction of $^{208}$Pb with 400A MeV $^{16}$O ions the inclusion of ground state correlations narrows the charge dispersion of spallation products by about 2 Z units. In view of the overall narrowing of the charge dispersion that accompanies the steepening of the sides of the valley of stability at lower mass numbers this effect would presumably be smaller, but still significant,for silver.

The discrepancy between the width of the isobaric yield distribution predicted by the cascade-evaporation model and that observed experimentally may thus be an indication of the importance of ground state correlations. Since the cascade model treats the target nucleus as a collection of quasi-free nucleons it does not incorporate such correlations, at least in the $t_r = \infty$ option of present interest. It has been pointed out[15] that the $t_r = 0$ option does include such correlations, albeit in a rather crude approximation. Within the rather large limits of uncertainty of the presently available $t_r = 0$ calculation, it does appear that somewhat narrower isotopic yield distributions are obtained by the use of this option. However, the distributions remain considerably broader than is observed experimentally.

Bertini et al.[47] have recently published the results of a high-energy intranuclear cascade calculation valid for incident protons up to 1000 GeV. Since there have been virtually no comparisons between spallation cross sections and the cascade-evaporation model in this energy regime it is of interest to compare our mass-yield curve for 300 GeV protons with this model. The Oak Ridge cascade code HECC-1[47,48] has been run in conjunction with an evaporation code based on the DFF formalism[44] for 300 GeV protons incident on $^{107,109}$Ag. The resulting mass-yield curve, binned in $\Delta A=5$ intervals, is compared with the experimental points in Fig. 7. With the exception of a sharp drop with decreasing A in the yields of products lying within 10 mass numbers from the target, the calculated mass yield curve is essentially flat. It therefore does not reproduce the continuous decrease in cross sections that is observed down to $A \sim 60$ and, moreover, underestimates the measured yields in the A=80-105 mass region by

about a factor-of-two. While approximate agreement is obtained in the A=20-80 mass region, the slope of the experimental mass yield curve is greater than that predicted. Furthermore, the agreement obtained at the lowest mass numbers is more apparent than real since the major fraction of the measured yield is due to fragmentation.[39] Although it appears that the calculation underestimates the value of the total reaction cross section, this shortcoming is only apparent. In fact, the calculated value of $\sigma_R$ is 1.11 barn, which is very close to our experimental value of 1.12 barn. What is not shown in Fig. 7 is that the calculated mass-yield extends below A=20, there being a contribution of 0.19 barn due to the formation of these very light residues.

The slope of the mass-yield curve is a measure of the excitation energy deposited in the residual nuclei by the intranuclear cascade. A flat mass yield is an indication that high-energy transfers are as probable as low- or medium-energy transfers. It thus appears that the HECC-1 code predicts the occurrence of high excitation energies with substantially greater probability than is observed experimentally. This shortcoming of the calculation may be a reflection of the assumptions concerning particle production built into the model. It is thus assumed that pion production in nucleon-nucleon collisions occurs via isobar formation and that the isobar decays at its point of formation. However, the relatively low average multiplicity of energetic secondary hadrons produced in p-nucleus collisions at high energies[49] suggests that this assumption is unfounded. It appears, instead, that the initial hadronic state produced in a high-energy collision does not decay to its final multi-particle state until it is well outside the struck nucleus. The resulting secondary particles

thus cannot interact inside the nucleus and so do not contribute to the excitation energy. The incorporation of this effect into the particle production model would presumably result in a lower average excitation energy of the struck nucleus and lead to better agreement with experiment.

C. Comparison with abrasion-ablation model

The abrasion-ablation model of the interaction of energetic heavy ions with nuclei[23] has been applied by Morrisey et al.[24] to the determination of the cross sections of target fragmentation products. The presently determined charge dispersion and mass-yield curve may be used to explore the validity of this formulation.

The model is analogous to the cascade-evaporation formalism in that it represents the interaction of a relativistic heavy ion with a complex nucleus as a two-step process: a prompt first step, abrasion, which corresponds to the cascade step, and a slower second step, ablation, which is identical to the evaporation step. Abrasion is a geometric model of the primary interaction. The projectile and target nuclei, which are represented as sharp spheres, make clean cuts through one another as a result of the collision. The number of nucleons sheared off from the target by this process, and hence the mass of the target residue, is calculated as a function of impact parameter by determining the intersecting volume of two spheres, corresponding to target and projectile. The excitation energy of the abraded residues is assumed to be equal to their excess surface energy, which results from their greater surface area relative to those of spherical nuclei of equal mass. The excitation energy is thus equal to the product of the excess surface area and the

nuclear surface energy coefficient. In the ablation step the excitation energy is dissipated by the evaporation of nucleons and light particles. The cross sections of the final products are obtained by summing the results over the impact parameter of the initial collision, each impact parameter being weighted by its geometric probability.

In order to perform this calculation it is necessary to make some assumptions about the distribution in atomic number of the abrasion products. Morrisey et al.[24] obtained this distribution on the assumption that the fluctuations in the number of protons removed when a given number of target nucleons is swept out by the projectile arises from zero point vibrations of the giant dipole resonance of the target nucleus. These workers postulate a Gaussian charge dispersion whose standard deviation is derived from the droplet model of the nucleus.[50] The final distribution of products is obtained from that following the abrasion step by use of the evaporation code OVERLAID ALICE.[51]

The mass-yield curve obtained for the interaction of $^{107,109}$Ag with $^{12}$C ions is displayed in Fig. 7. The curve is terminated at A $\sim$ 60 since at lower mass numbers it turns up in an unphysical way due to the onset of near-central collisions.[24] The calculated mass-yield curve fits the experimental points in the A $\sim$ 60-90 mass region remarkably well. However, at higher mass numbers the calculation overestimates the isobaric cross sections. In a somewhat different formulation of the abrasion-ablation model, Oliveira,Donangelo, and Rasmussen[52] also noted that the model overestimated the mass-yield curve in the vicinity of the target. Following an earlier suggestion by Hüfner, Schäfer, and Schürmann,[53] these workers assumed that this discrepancy was due to the neglect of final state

interactions. These interactions are those between some of the outgoing abraded nucleons and the remaining spectator nucleons. Since the former tend to move perpendicular to the beam direction they can scatter off the spectator nucleons on their way out of the nucleus. The resulting energy transfer increases the excitation energy of the abraded nucleus. This effect appears to be particularly important for abrasion products that have only a few less nucleons than the target and so have very little excess surface energy. The incorporation of this effect reduces the calculated cross sections of products near the target and leads to improved agreement with experiment.[52] While this model has not been compared with the present data, a similar improvement should be obtained. In addition, the increase in the excitation energy of the abraded nuclei must lead to larger cross sections for products far from the target and, in the case of present interest, should lead to an extension of the calculated mass-yield curve below $A \sim 60$. Since the departures from factorization only become noticeable at $A \sim 40$, one might expect target fragmentation to populate this extended mass region. While the inclusion of final state interactions thus appears to improve the agreement with experiment, it becomes necessary to sacrifice the remarkable simplicity that makes the abrasion-ablation model so attractive. The inclusion of nucleon-nucleon scattering processes thus leads to a more hybrid model, incorporating intra-nuclear cascade as well as strictly geometric features.

The isotopic yield distributions obtained for As, Y, and Pd are compared with the experimental values in Fig. 8. The results for As and Y are in good agreement with the data indicating that the giant dipole resonance model of the primary charge dispersion is valid for interactions

in which considerable abrasion occurs. In contrast, the calculation does not fit the distribution of palladium isotopes. The model thus severely underestimates the number of emitted neutrons. An examination of the isobaric yield distribution in this mass region indicates that the calculation considerably underestimates its width. For instance, at A=100 the full-width is 1.1 Z units compared to the experimental value of 1.9. It thus appears that the giant dipole resonance model is not suitable for the most peripheral interactions, in which very small mass loss occurs. In their calculation of the yields of products from the interaction of heavy ions with light element targets, Oliveira, Donangelo, and Rasmussen[52] assumed that the proton and neutron distributions of the struck nucleus were completely uncorrelated. The charge dispersion of the abraded nuclei is then given by the hypergeometric function. This model has been shown[24,52] to lead to much broader distributions than the giant dipole resonance model. While such large widths are unrealistic for products far removed from a silver target nucleus, they may constitute a better representation for the most peripheral collisions.

The geometric nature of the abrasion-ablation model implies a correspondence between the average impact parameter, $\bar{b}$, of the collision and the mass number of the final products. This correspondence is made explicit in Fig. 5. It is apparent that the mass number of the products decreases as $\bar{b}$ decreases. In the vicinity of $\bar{b} = 3$, target and projectile overlap at their half-density points and the model becomes unrealistic at smaller impact parameters. At this value of $\bar{b}$ the mass number of the target residue is in the vicinity of 55. While the terms "peripheral" and "central" are qualitative, it seems reasonable to conclude that

when the impact parameter becomes as small as the difference between the half-density radii of target and projectile, it no longer makes sense to refer to the collisions as "peripheral." In view of the fact that the observed deviations from factorization occur not far from this mass number, the model lends support to the notion that they are associated with the onset of central collisions. The incorporation of final-state interactions would presumably improve this correspondence.

## V. Conclusions

The determination of approximately 100 formation cross sections of radionuclides from the interaction of silver with 2.1A GeV $^{12}C$ ions and 300 GeV protons, and the development of a well tailored parametrization of these data, have enabled us to perform a detailed comparison of the interaction of these two projectiles with a medium A target in the energy regime in which limiting fragmentation appears to be valid. The charge dispersions were found to be closely comparable and the mass yield curves obey factorization down to $A \sim 40$. However, products of lower mass number have enhanced yields in $^{12}C$-induced reactions, the enhancement below $A \sim 30$ relative to the ratio of reaction cross sections being a factor-of-two or more. The formation of these products is shown to be associated with central collisions.

The results have been compared with several reaction models. Monte Carlo cascade-evaporation calculations[15] predict a mass-yield curve that is in excellent agreement with the curve obtained for $^{12}C$ ions. This agreement extends down to $A \sim 40$ indicating that $^{12}C$ ions are effective in transferring the high excitation energies needed to form these products

by spallation. Since the cascade model is based on the assumption that the interaction between the two nuclei consists of a series of collisions between individual nucleons, the agreement is an indication that most of the reaction channels do not involve collective interactions. A more detailed comparison, involving several series of isotopic cross sections, indicates that the calculated charge dispersions are considerably broader than is observed. This discrepancy can be explained on the assumption that there are ground-state correlations between neutrons and protons that are preserved in the intra-nuclear cascade as well as in the subsequent evaporation phase.

A similar comparison of the mass-yield curve obtained in proton reactions with the Oak Ridge HECC-1 cascade code[47] run for 300 GeV protons yields less satisfactory agreement. The calculated curve is thus much flatter than the experimental one indicating that the model overestimates the excitation energies of the struck nuclei. This overestimation may be due to simplifications in the multiparticle production process associated with the assumption of instantaneous decay of excited hadronic states.

The mass yield curve from the interaction of $^{12}C$ ions with silver, as well as selected isotopic yield distributions, have been compared with an abrasion-ablation model[23] calculation in which the charge dispersion of the abraded nuclei was obtained on the assumption of neutron-proton correlations based on the giant dipole resonance model.[24] The isotopic yield distributions are in excellent agreement with experiment, except in the vicinity of the target, where they are too narrow. This agreement is a further indication that the discrepancy observed between the isotopic yield distributions and the Monte Carlo simulation can be attributed to the neglect of these correlations in this calculation. The mass yield curve

predicted by the abrasion-ablation model is in moderately good agreement with experiment except that it overestimates the yields of products close to the target and indicates that the target fragmentation cross section is used up by A $\sim$ 60 instead of extending some additional twenty mass numbers to A $\sim$ 40. These discrepancies indicate that the excitation energy spectrum of the abraded nuclei must be shifted towards higher values than predicted by this model. The incorporation of final state interactions[52] appears to be an improvement in this respect.

The cooperation of Dr. F. Lothrop and the operating staff of the Bevalac is gratefully acknowledged. We wish to thank Dr. W. Everette and D. Murphy for assistance with the use of the ion chamber. We are grateful to Professors G. T. Seaborg and S. M. Markowitz for making their counting room facilities available to us. D. Lee and Dr. R. Otto were most helpful in connection with the use of these facilities. We wish to thank Dr. S. Baker for the use of the Fermilab counting room. Thanks are due to Professor Z. Fraenkel for performing the Monte Carlo cascade-evaporation calculations for $^{12}$C ions, to Dr. T. A. Gabriel for the proton Monte Carlo calculations, to Dr. D. J. Morrisey for the abrasion-ablation calculations, and to Dr. J. B. Cumming for a copy of his cross section code. We acknowledge the financial support of the U.S. Department of Energy.

## References


1. H. H. Heckman, D. E. Greiner, P. J. Lindstrom, and F. S. Bieser, Phys. Rev. Lett. 28, 926 (1972).
2. D. E. Greiner, P. J. Lindstrom, H. H. Heckman, B. Cork, and F. S. Bieser, Phys. Rev. Lett. 35, 152 (1975).
3. H. H. Heckman, D. E. Greiner, P. J. Lindstrom, and H. Shwe, Phys. Rev. C17, 1735 (1978).
4. J. B. Cumming, P. E. Haustein, R. W. Stoenner, L. Mausner, and R. A. Naumann, Phys. Rev. C10, 739 (1974).
5. J. B. Cumming, R. W. Stoenner, and P. E. Haustein, Phys. Rev. C14, 1554 (1976).
6. W. Loveland, R. J. Otto, D. J. Morrissey, and G. T. Seaborg, Phys. Rev. Lett. 39, 320 (1977).
7. W. Loveland, R. J. Otto, D. J. Morrissey and G. T. Seaborg, Phys. Lett. 69B, 284 (1977).
8. J. B. Cumming, P. E. Haustein, T. J. Ruth, and G. J. Virtes, Phys. Rev. C17, 1632 (1978).
9. J. D. Sullivan, P. B. Price, H. J. Crawford, and M. Whitehead, Phys. Rev. Lett. 30, 136 (1973).
10. H. J. Crawford, P. B. Price, J. Stevenson, and L. W. Wilson, Phys. Rev. Lett. 34, 329 (1975).
11. A. M. Poskanzer, R. G. Sextro, A. M. Zebelman, H. H. Gutbrod, A. Sandoval, and R. Stock, Phys. Rev. Lett. 35, 1701 (1975).
12. J. Gosset, H. H. Gutbrod, W. G. Meyer, A. M. Poskanzer, A. Sandoval, R. Stock, and G. D. Westfall, Phys. Rev. C16, 629 (1977).
13. H, W. Bertini, T. A. Gabriel, and R. T. Santoro, Phys. Rev. C9, 522 (1974).

14. A. A. Amsden, J. N. Ginocchio, F. H. Harlow, J. R. Nix, M. Danos, E. C. Halbert, and R. K. Smith, Jr., Phys. Rev. Lett. 38, 1055 (1977).

15. Y. Yariv and Z. Fraenkel, to be published.

16. See the review by H. Bøggild and T. Ferbel, Annu. Rev. Nucl. Sci. 24, 451 (1974).

17. S. Barshay, C. B. Dover, and J. P. Vary, Phys. Rev. C11, 360 (1975).

18. P. J. Karol, Phys. Rev. C11, 1203 (1975).

19. S. Katcoff and J. Hudis, Phys. Rev. Lett. 28, 1066 (1972).

20. S. Katcoff, H. R. Fickel, and A. Wyttenbach, Phys. Rev. 166, 1147 (1968).

21. G. English, N. T. Porile, and E. P. Steinberg, Phys. Rev. C10, 2268 (1974).

22. G. English, Y. W. Yu, and N. T. Porile, Phys. Rev. C10, 2281, (1974).

23. J. D. Bowman, W. J. Swiatecki, and C. F. Tsang, Lawrence Berkeley Laboratory Report LBL-2908, 1973 (unpublished).

24. D. J. Morrissey, W. R. Marsh, R. J. Otto, W. Loveland, and G. T. Seaborg, Phys. Rev. C18, 1267 (1978).

25. C. R. Rudy and N. T. Porile, Phys. Lett. 59B, 240 (1975).

26. D. Murphy, private communication.

27. J. B. Cumming, Annu. Rev. Nucl. Sci. 13, 261 (1963).

28. W. Everette, private communication.

29. J. T. Routti and S. G. Prussin, Nucl. Instr. 72, 125 (1969).

30. J. B. Cumming, National Academy of Sciences Report No. NAS-NS-3107, 1962 (unpublished), p. 25.

31. W. W. Bowman and K. W. MacMurdo, Nucl. Data 13, 90 (1974).

32. Nuclear Data Sheets, Vols. 16-22, 1975-77.

33. A. H. Jaffey, Rev. Sci. Instr. 25, 349 (1954).

34. G. J. McCallum and G. E. Coote, Nucl. Instr. 130, 189 (1975).

35. S. B. Kaufman, M. W. Weisfield, E. P. Steinberg, B. D. Wilkins, and D. Henderson, Phys. Rev. C14, 1121 (1976).

36. E. K. Hyde, G. W. Butler, and A. M. Poskanzer, Phys. Rev. C4, 1759 (1971); R. G. Korteling, C. R. Toren, and E. K. Hyde, Phys. Rev. C7, 1611 (1973).

37. A. M. Poskanzer, G. W. Butler, and E. K. Hyde, Phys. Rev. C3, 882 (1971).

38. G. Rudstam, Z. Naturforschg. 219, 1027 (1966).

39. J. B. Cumming, S. Katcoff, N. T. Porile, S. Tanaka, and A. Wyttenbach, Phys. Rev. 134, B1262 (1964).

40. J. Hudis and S. Katcoff, Phys. Rev. 180, 1122 (1969).

41. A. Ashmore, G. Cocconi, A. N. Diddens, and A. M. Wetherell, Phys. Rev. Lett. 5, 576 (1960).

42. K. Chen, Z. Fraenkel, G. Friedlander, J. R. Grover, J. M. Miller, and Y. Shimamoto, Phys. Rev. 166, 949 (1968).

43. G. D. Harp, Phys. Rev. C10, 2387 (1974).

44. I. Dostrovsky, Z. Fraenkel, and G. Friedlander, Phys. Rev. 116, 683 (1959).

45. N. T. Porile and L. B. Church, Phys. Rev. 133, B310 (1964).

46. J. P. Bondorf, G. Fai, and O. B. Nielsen, Phys. Rev. Lett. 41, 391 (1978).

47. H. W. Bertini, A. H. Culkowski, O. W. Hermann, N. B. Gove, and M. P. Guthrie, Phys. Rev. C17, 1382 (1978).

48. T. A. Gabriel, private communication.

49. W. Busza, Acta Phys. Pol. B8, 333 (1977)

50. W. D. Myers, W. J. Swiatecki, T. Kodama, L. J. El-Jaick, and E. R. Hilf, Phys. Rev. C15, 2032 (1977).

51. M. Blann, USERDA Report No. COO-3494-29, Rochester, N.Y. (1976) unpublished.

52. L. F. Oliveira, R. Donangelo, and J. O. Rasmussen, Lawrence Berkeley Laboratory Report LBL-7731 (1978); submitted to Phys. Rev. C.

53. J. Hüfner, K. Schäfer, and B. Schürmann, Phys. Rev. C12, 1888 (1975).

Table I. Cross sections for the production of radionuclides in the interaction of silver with 25.2 GeV $^{12}C$ ions and 300 GeV protons.

| Nuclide | Type of yield | $\sigma(^{12}C)$ (mb) | $\sigma(P)$ (mb) |
|---|---|---|---|
| $^{7}Be$ | I | 82.6±9.7 | 18.7±1.3 |
| $^{22}Na$ | C+ | 17.3±1.5 | 2.37±0.10 |
| $^{24}Na$ | C- | 14.8±0.9 | 5.22±0.14 |
| $^{27}Mg$ | C- | -- | 1.54±0.09 |
| $^{28}Mg$ | C- | 2.10±0.15 | 0.70±0.04 |
| $^{29}Al$ | C- | 8.13±1.26 | 2.28±0.13 |
| $^{38}Cl$ | C- | 3.34±0.52 | 1.18±0.04 |
| $^{39}Cl$ | C- | 0.88±0.22 | 0.60±0.08 |
| $^{41}Ar$ | C- | 1.38±0.13 | 0.66±0.02 |
| $^{42}K$ | I | 4.06±0.46 | 2.24±0.15 |
| $^{43}K$ | C- | 2.02±0.16 | 1.31±0.05 |
| $^{43}Sc$ | C+ | 2.16±0.23 | 1.87±0.20 |
| $^{44}Sc$ | I | 2.70±0.12 | 1.71±0.08 |
| $^{44}Sc^{m}$ | I | 4.36±0.17 | 2.28±0.07 |
| $^{46}Sc$ | I | 8.08±0.76 | 3.18±0.06 |
| $^{47}Ca$ | C- | -- | 0.09±0.01 |
| $^{47}Sc$ | I | 3.40±0.23 | 1.74±0.18 |
| $^{48}Sc$ | I | 1.02±0.09 | 0.55±0.04 |
| $^{48}V$ | C+ | 6.49±0.69 | 3.06±0.06 |
| $^{49}Cr$ | C+ | 0.70±0.05 | 0.63±0.04 |
| $^{52}Mn$ | I | 3.98±0.22 | 2.19±0.10 |
| $^{52}Mn^{m}$ | C+ | -- | 0.44±0.04 |
| $^{54}Mn$ | I | 8.63±0.90 | 4.70±0.30 |
| $^{55}Co$ | C+ | 0.55±0.14 | 0.33±0.04 |

| Nuclide | Type of yield | $\sigma(^{12}C)$ (mb) | $\sigma(P)$ (mb) |
|---|---|---|---|
| $^{56}Mn$ | C- | 2.19±0.20 | 1.07±0.03 |
| $^{56}Co$ | C+ | 3.43±0.44 | 1.49±0.07 |
| $^{57}Co$ | C+ | 6.11±1.10 | 4.41±0.18 |
| $^{58}Co$ | I | 10.6±1.1 | 5.80±0.20 |
| $^{59}Fe$ | C- | 2.28±1.07 | 0.59±0.03 |
| $^{60}Co$ | I | --- | 1.9±0.1 |
| $^{60}Cu$ | C+ | 1.45±0.22 | 0.61±0.08 |
| $^{65}Zn$ | C+ | 16.1±1.1 | 7.39±0.48 |
| $^{66}Ga$ | C+ | 7.78±0.49 | 4.12±0.20 |
| $^{67}Ge$ | C+ | 1.29±0.21 | 1.12±0.04 |
| $^{69}Ge$ | C+ | 9.46±0.75 | 6.71±0.21 |
| $^{69}Zn^{m}$ | I | 0.57±0.07 | 0.61±0.06 |
| $^{70}As$ | C+ | 4.27±0.45 | 2.54±0.33 |
| $^{71}As$ | C+ | 10.1±0.6 | 6.32±0.90 |
| $^{72}As$ | I | 12.4±0.6 | 6.57±0.98 |
| $^{73}Se$ | PC+ | 8.63±0.40 | 5.87±0.10 |
| $^{74}As$ | I | 4.34±0.29 | 2.42±0.05 |
| $^{74}Br^{m}$ | I | --- | 1.45±0.11 |
| $^{75}Se$ | C+ | 19.0±1.0 | 11.6±0.2 |
| $^{75}Br$ | C+ | 8.07±0.53 | 5.66±0.10 |
| $^{76}Br$ | I | --- | 6.79±1.05 |
| $^{76}Kr$ | C+ | 2.39±0.16 | 1.76±0.19 |
| $^{77}Br$ | C+ | 14.5±1.0 | 9.11±0.23 |
| $^{77}Kr$ | C+ | 7.80±0.81 | 5.52±0.31 |
| $^{79}Kr$ | C+ | 14.6±1.2 | 10.4±0.5 |
| $^{79}Rb$ | C+ | 7.03±0.36 | --- |
| $^{81}Rb$ | PC+ | 16.2±4.6 | 14.0±0.7 |

| Nuclide | Type of yield | $\sigma(^{12}C)$ (mb) | $\sigma(P)$ (mb) |
|---|---|---|---|
| $^{82}Rb^{m}$ | I | 7.71±0.31 | 5.60±0.28 |
| $^{82}Sr$ | C+ | --- | 7.38±0.34 |
| $^{83}Rb$ | C+ | 25.4±1.3 | 14.7±0.4 |
| $^{83}Sr$ | C+ | 16.3±1.0 | 10.9±0.3 |
| $^{84}Rb^{m}$ | I | 1.36±0.16 | 1.18±0.06 |
| $^{84}Rb^{m+g}$ | I | 3.82±0.52 | 1.50±0.03 |
| $^{84}Y$ | C+ | 6.42±0.50 | 4.77±0.14 |
| $^{85}Y$ | PC+ | --- | 7.76±0.80 |
| $^{85}Zr$ | PC+ | 1.52±0.23 | 1.06±0.10 |
| $^{86}Y^{m}$ | I | 9.89±0.61 | 7.05±0.14 |
| $^{86}Y^{m+g}$ | I | 16.3±1.4 | 9.57±0.30 |
| $^{86}Zr$ | C+ | 8.98±0.22 | 5.93±0.36 |
| $^{87}Y$ | I | --- | 0.57±0.32 |
| $^{87}Y^{m}$ | C+ | 25.5±1.6 | 15.9±0.8 |
| $^{88}Y$ | I | 7.85±0.85 | 3.11±0.20 |
| $^{88}Zr$ | C+ | 29.4±2.3 | 14.7±0.2 |
| $^{88}Nb$ | PC+ | 3.36±0.52 | 2.65±0.18 |
| $^{89}Zr$ | C+ | 29.5±1.6 | 15.8±0.4 |
| $^{89}Nb^{g}$ | ? | 1.62±0.16 | 0.83±0.02 |
| $^{89}Nb^{m}$ | ? | 27.0±1.9 | 9.5±1.0 |
| $^{90}Y^{m}$ | I | 0.47±0.06 | 0.37±0.03 |
| $^{90}Nb$ | I | 23.3±1.0 | 13.2±0.6 |
| $^{90}Mo$ | C+ | 4.80±0.28 | 3.32±0.16 |
| $^{92}Nb^{m}$ | I | 5.24±0.24 | --- |
| $^{92}Tc$ | C+ | --- | 2.01±0.13 |
| $^{93}Mo^{m}$ | I | 5.28±0.40 | 2.99±0.11 |
| $^{93}Tc$ | PC+ | 13.7±1.3 | 6.56±0.17 |

| Nuclide | Type of yield | $\sigma(^{12}C)$ (mb) | $\sigma(P)$ (mb) |
|---|---|---|---|
| $^{94}Tc$ | I | 14.1±0.6 | 7.65±0.39 |
| $^{94}Tc^{m}$ | C+ | 6.44±0.70 | 2.13±0.21 |
| $^{95}Nb^{m}$ | I | 11.7±1.2 | --- |
| $^{95}Tc$ | C+ | 24.3±1.6 | --- |
| $^{95}Ru$ | C+ | 9.98±1.35 | 5.40±0.70 |
| $^{96}Nb$ | I | 1.41±0.17 | 0.57±0.14 |
| $^{96}Tc$ | I | 12.3±0.6 | 7.38±0.19 |
| $^{96}Rh$ | PC+ | 2.51±0.42 | 0.75±0.04 |
| $^{97}Ru$ | C+ | 24.7±0.8 | 15.7±0.6 |
| $^{97}Rh^{m}$ | ? | 5.93±0.25 | 3.94±0.15 |
| $^{98}Rh$ | I | 11.9±2.3 | --- |
| $^{98}Pd$ | C+ | 1.91±0.22 | 1.05±0.06 |
| $^{99}Rh$ | I | 4.34±0.36 | 2.91±0.11 |
| $^{99}Rh^{m}$ | I | 17.2±1.1 | 8.42±0.45 |
| $^{99}Pd$ | C+ | 3.63±0.21 | 2.94±0.11 |
| $^{100}Rh$ | I | 21.3±1.4 | 12.4±0.3 |
| $^{100}Pd$ | C+ | 8.47±0.93 | 5.78±0.25 |
| $^{101}Rh^{m}$ | I | 26.1±2.8 | --- |
| $^{101}Pd$ | C+ | 22.0±1.3 | 12.9±0.4 |
| $^{102}Rh$ | I | 8.46±2.17 | 2.88±0.46 |
| $^{102}Rh^{m}$ | I | 9.86±3.32 | 5.6±1.0 |
| $^{102}Ag$ | PC+ | 5.15±0.48 | 2.71±0.12 |
| $^{103}Ru$ | C- | 1.12±0.31 | 0.75±0.03 |
| $^{103}Ag$ | C+ | 14.5±0.8 | 13.0±0.8 |
| $^{104}Ag$ | PC+ | 18.0±1.1 | --- |
| $^{104}Ag^{m}$ | C+ | 4.20±0.81 | 1.94±0.42 |
| $^{105}Rh$ | C- | 5.32±0.92 | 3.96±0.49 |
| $^{105}Ag$ | C+ | 44.4±3.5 | 25.0±0.9 |

| Nuclide | Type of yield | $\sigma(^{12}C)$ (mb) | $\sigma(P)$ (mb) |
|---|---|---|---|
| $^{106}Ru$ | C- | 7.68±3.03 | --- |
| $^{106}Rh^{m}$ | I | --- | 1.36±0.16 |
| $^{106}Ag^{m}$ | I | 20.7±1.7 | 11.4±0.6 |

Table 2. Parameters obtained from the fit of Eqs. (1) and (2) to the cross sections of A=20-100 products from the interaction of silver with high-energy $^{12}C$ ions and protons.

| Parameter | $^{12}C$ | Protons |
|---|---|---|
| $\alpha_1$ | 6.31±0.24 | 2.58±0.13 |
| $\alpha_2$ | -0.198±0.012 | $-(4.89\pm0.68)\times10^{-2}$ |
| $\alpha_3$ | $(3.06\pm0.20)\times10^{-3}$ | $(8.20\pm1.14)\times10^{-4}$ |
| $\alpha_4$ | $-(1.41\pm0.10)\times10^{-5}$ | $-(3.32\pm0.61)\times10^{-6}$ |
| $\alpha_5$ | -1.46±0.24 | -1.78±0.15 |
| $\alpha_6$ | $-(8.99\pm7.12)\times10^{-3}$ | $(3.14\pm4.50)\times10^{-4}$ |
| $\alpha_7$ | $(1.58\pm0.51)\times10^{-4}$ | $(6.64\pm3.28)\times10^{-5}$ |
| $\alpha_8$ | 1.65±0.06 | 1.48±0.03 |
| $\alpha_9$ | 0.480±0.000 | 0.481±0.000 |
| $\alpha_{10}$ | $-(2.99\pm0.06)\times10^{-4}$ | $-(2.92\pm0.03)\times10^{-4}$ |

## Figures

Fig. 1. Ratio of cross sections obtained for 250 and 75 μm thick silver targets bombarded by 25.2 GeV $^{12}C$ ions. Open points, neutron-excessive nuclides; closed points, neutron deficient nuclides. The lines are the result of a least-squares fit described in the text.

Fig. 2. Comparison of the fitted fractional isobaric yield distribution at A=70 (curve) and the data points adjusted to A=70 (see text). The different symbols identify the product mass region: o, A=21-40; ●, A=41-60; Δ, A=61-80; ▲, A=81-100. The left panel presents the comparison of the proton data and the right, that of the $^{12}C$ results.

Fig. 3. Comparison of the fitted mass-yield curves with the data. The points are the experimental isobaric cross sections with estimates of the unmeasured contributions obtained from the fitting procedure described in the text. The different symbols indicate the fraction of the isobaric yield that was measured: o, >50%; Δ, 20-50%; □, 10-20%. The open points refer to proton bombardments and the closed points to $^{12}C$. The curves are based on Eqs. (1) and (2). The dashed extensions above A=100 are based on a separate analysis of the data in this mass region. The crosses represent data from earlier proton work [ref. 20].

Fig. 4. Mass dependence of $Z_p/A$ (top panel) and of the width of the isobaric yield distributions (bottom). Solid lines, proton reactions; dashed, $^{12}C$. The dotted curve shows the variation of $Z_A/A$. The crosses represent results for incident protons from ref. 20.

Fig. 5. Constant cross section contours for the reactions of silver with $^{12}C$ ions. Contours corresponding to 25, 12, and 6 mb are shown. The dashed

line represents the smoothened behavior of $Z_A$. The crosses mark the location of the target. The arrows and associated numbers indicate the mass number. The diagonal scale gives the average impact parameter of the collisions leading to products of indicated A value, as obtained from the abrasion-ablation model [ref. 24].

Fig. 6. Ratios of $^{12}C$ to proton cross sections. The points are based on the data in Table 1. The curve is the ratio of $\sigma_A$ values obtained from the cross section parametrization. The horizontal lines represent two estimates of the ratio of total reaction cross sections.

Fig. 7. Comparison of mass-yield curves with Monte Carlo and abrasion-ablation calculations. Closed points, $^{12}C$ isobaric cross sections from Fig. 3; solid histogram, Monte Carlo cascade evaporation calculation for 1 GeV A $^{12}C$ plus silver [ref. 15]; dashed curve, abrasion-ablation calculation [ref. 24]; open points, proton isobaric cross sections from Fig. 3; dashed histogram, Monte Carlo cascade-evaporation calculation for 300 GeV protons plus silver [refs. 47,48].

Fig. 8. Comparison of isotopic yields of various elements formed in $^{12}C$ reactions with calculations. Points, experimental independent cross sections (corrected for progenitor yield where necessary); solid lines, Monte Carlo cascade-evaporation calculation (2 $\sigma$ interval centered on calculated cross sections) [ref. 15]; dashed line, abrasion-ablation calculation [ref. 24].

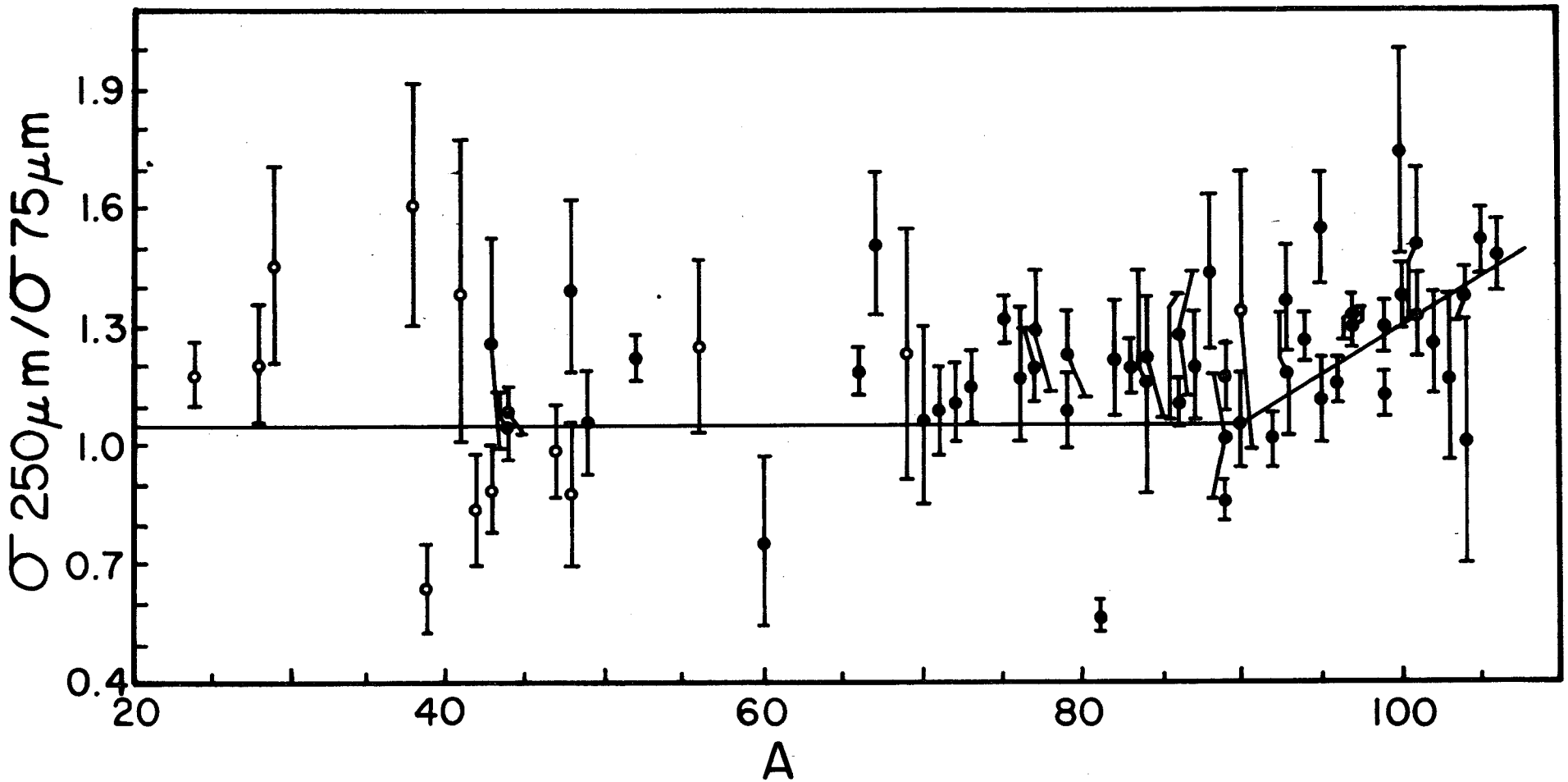


Perlo et al

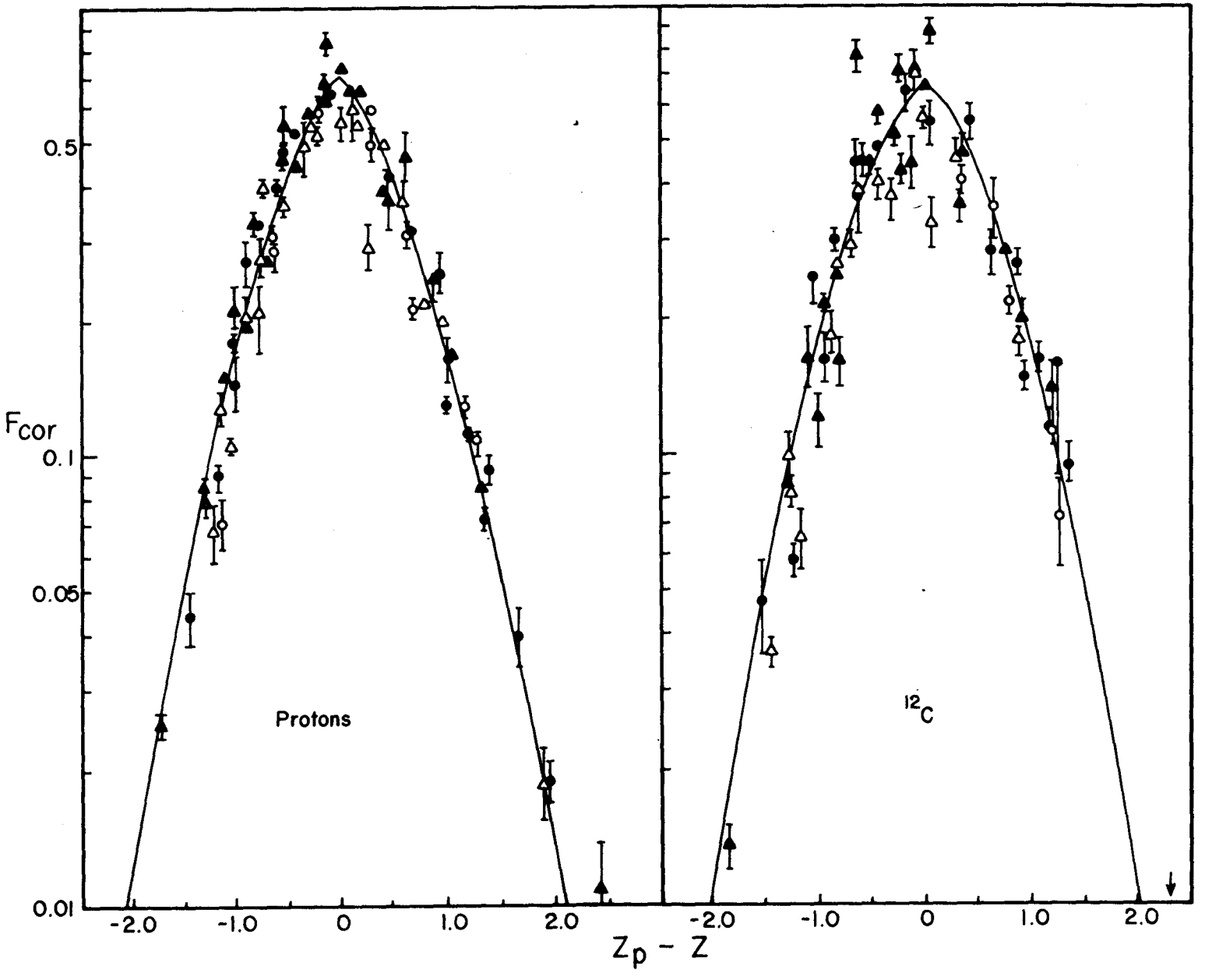
0.5
0.1
0.05
0.01
$F_{cor}$
Protons
$^{12}C$
-2.0
-1.0
0
1.0
2.0
$Z_p - Z$

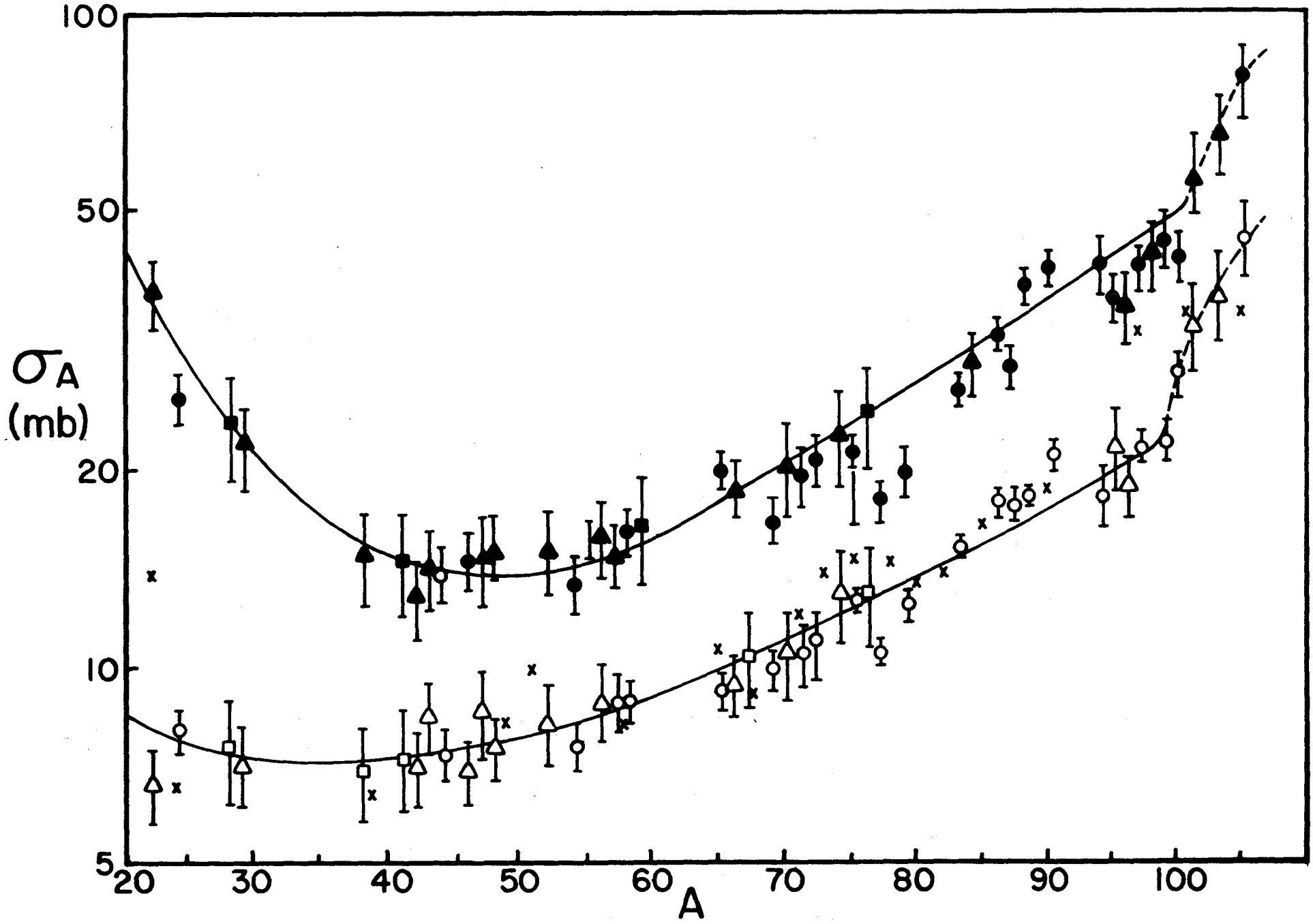


Fig 3
Pavlee e

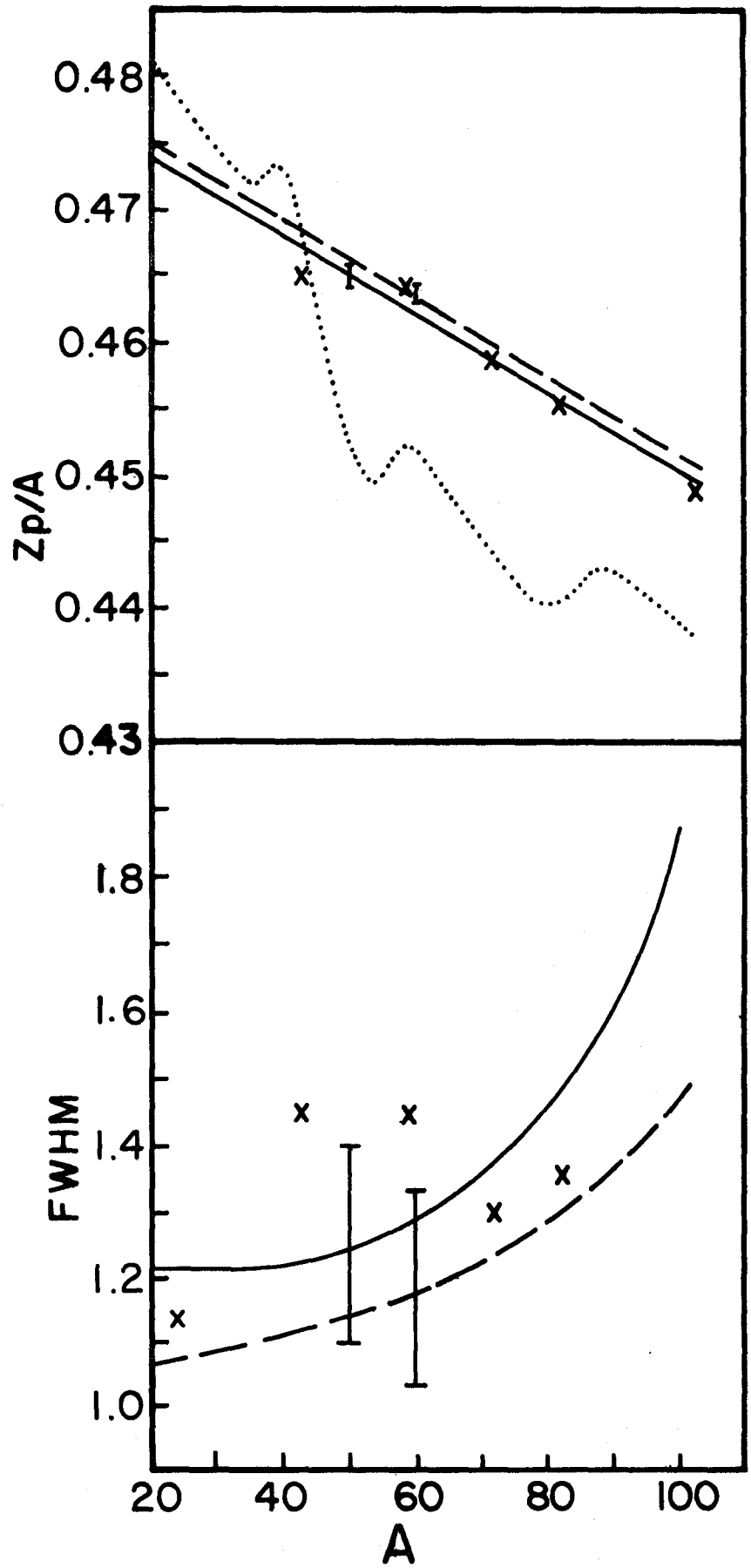


Price et al Fig 4

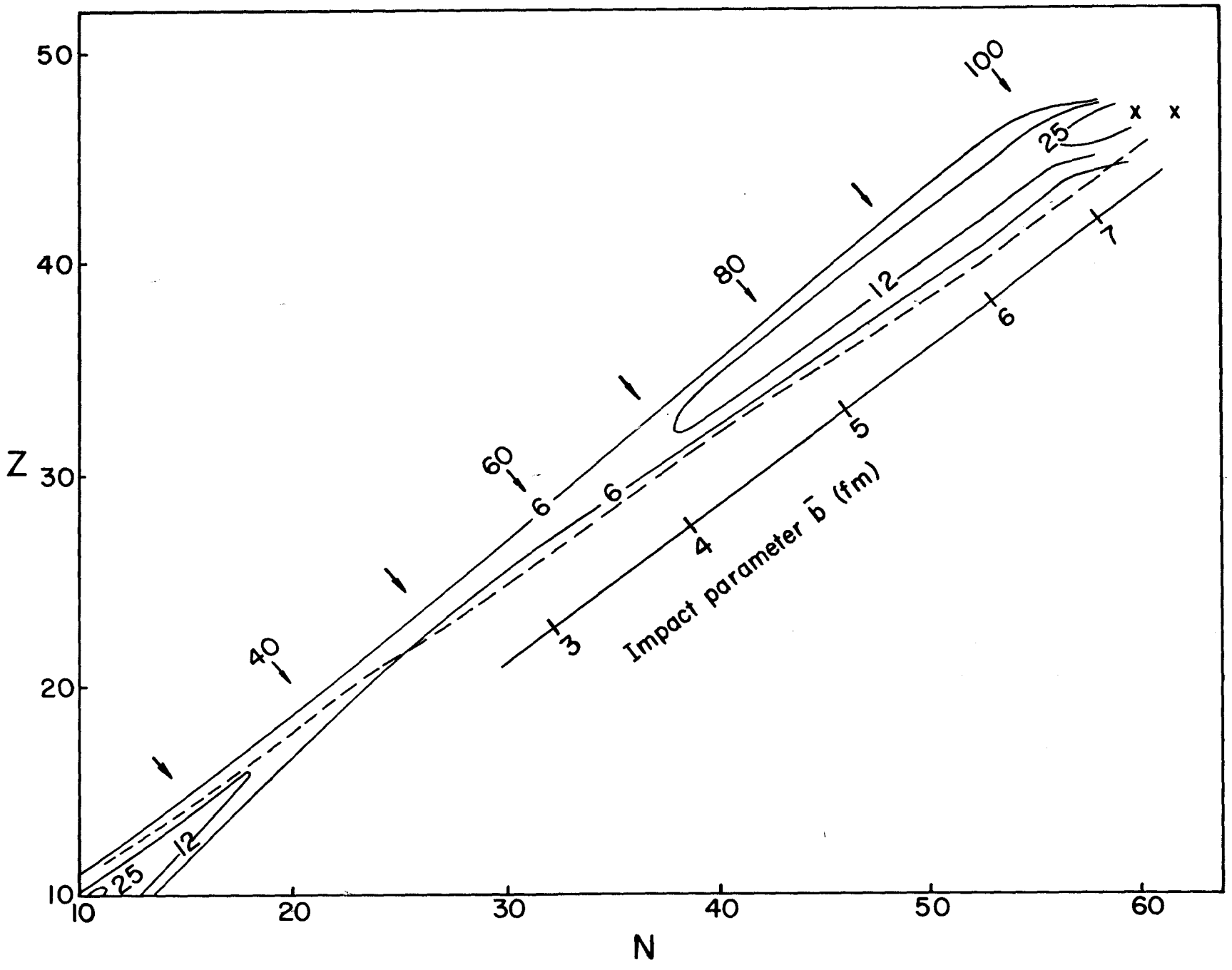
Z
N
10
20
30
40
50
60
100
80
60
40
25
12
6
7
5
4
3
Impact parameter $\bar{b}$ (fm)

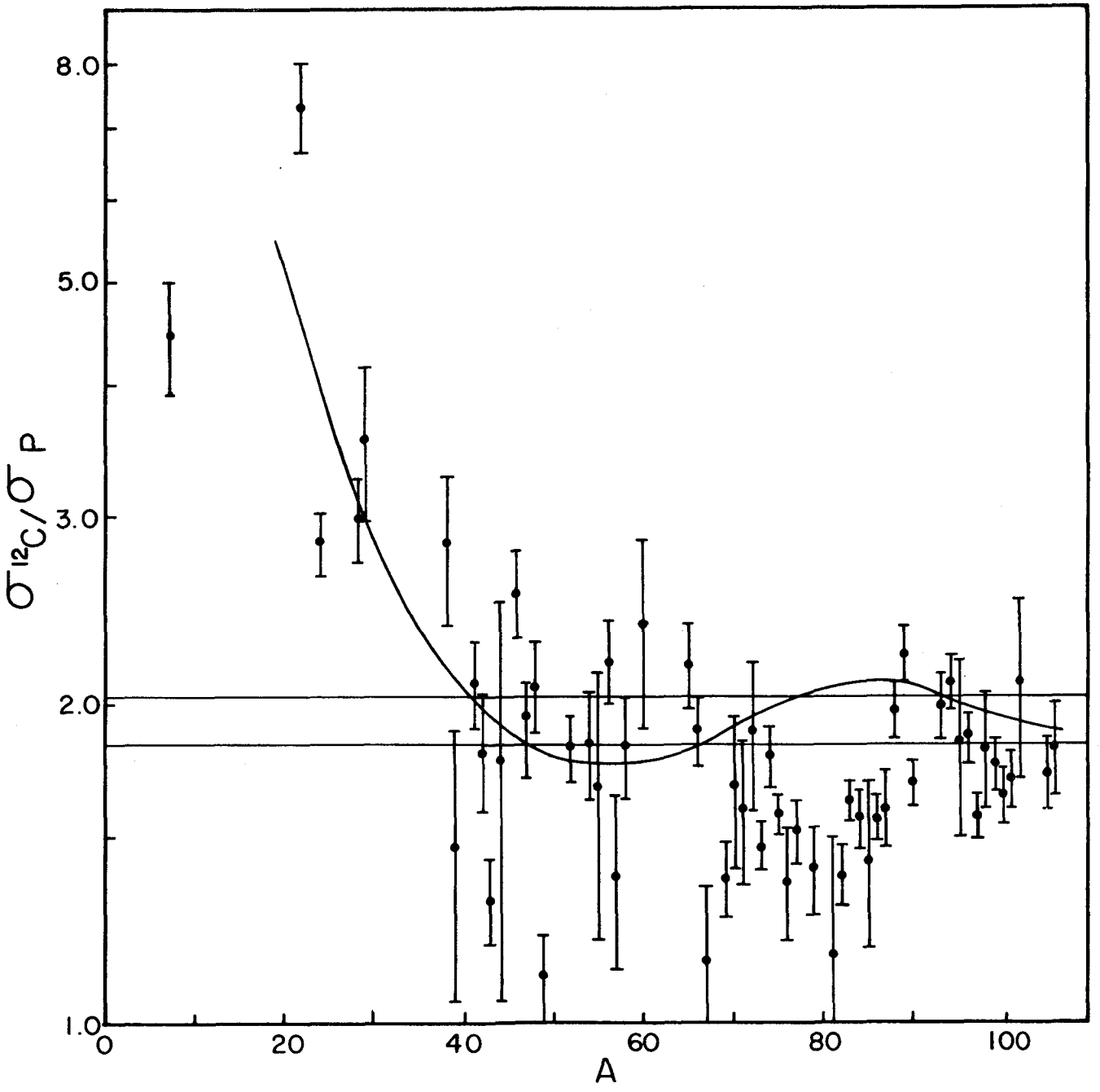
8.0
5.0
3.0
2.0
1.0
0
20
40
60
80
100
A
$\sigma_{^{12}C}/\sigma_P$

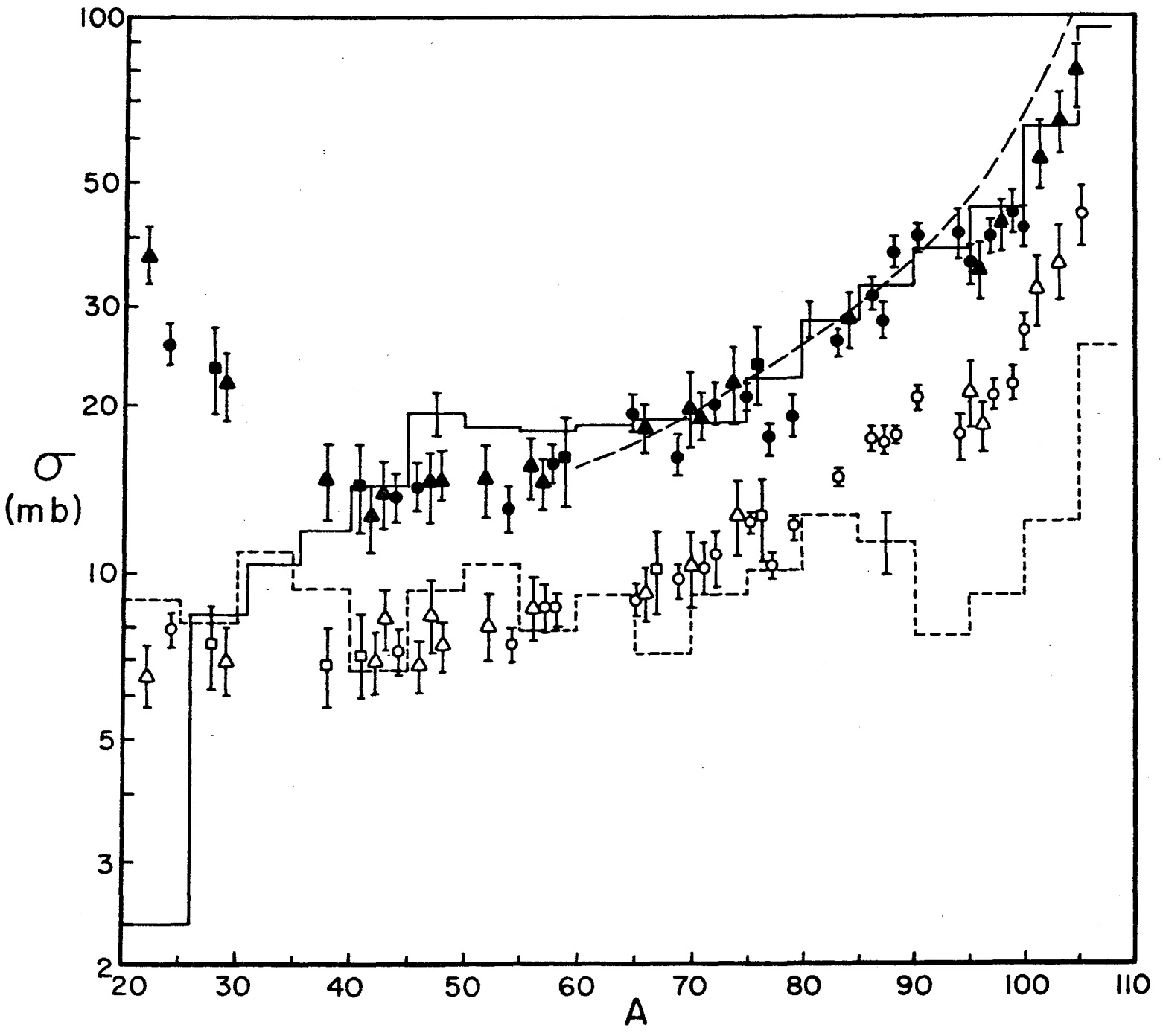
100
50
30
20
10
5
3
2
σ
(mb)
20
30
40
50
60
70
80
90
100
110
A

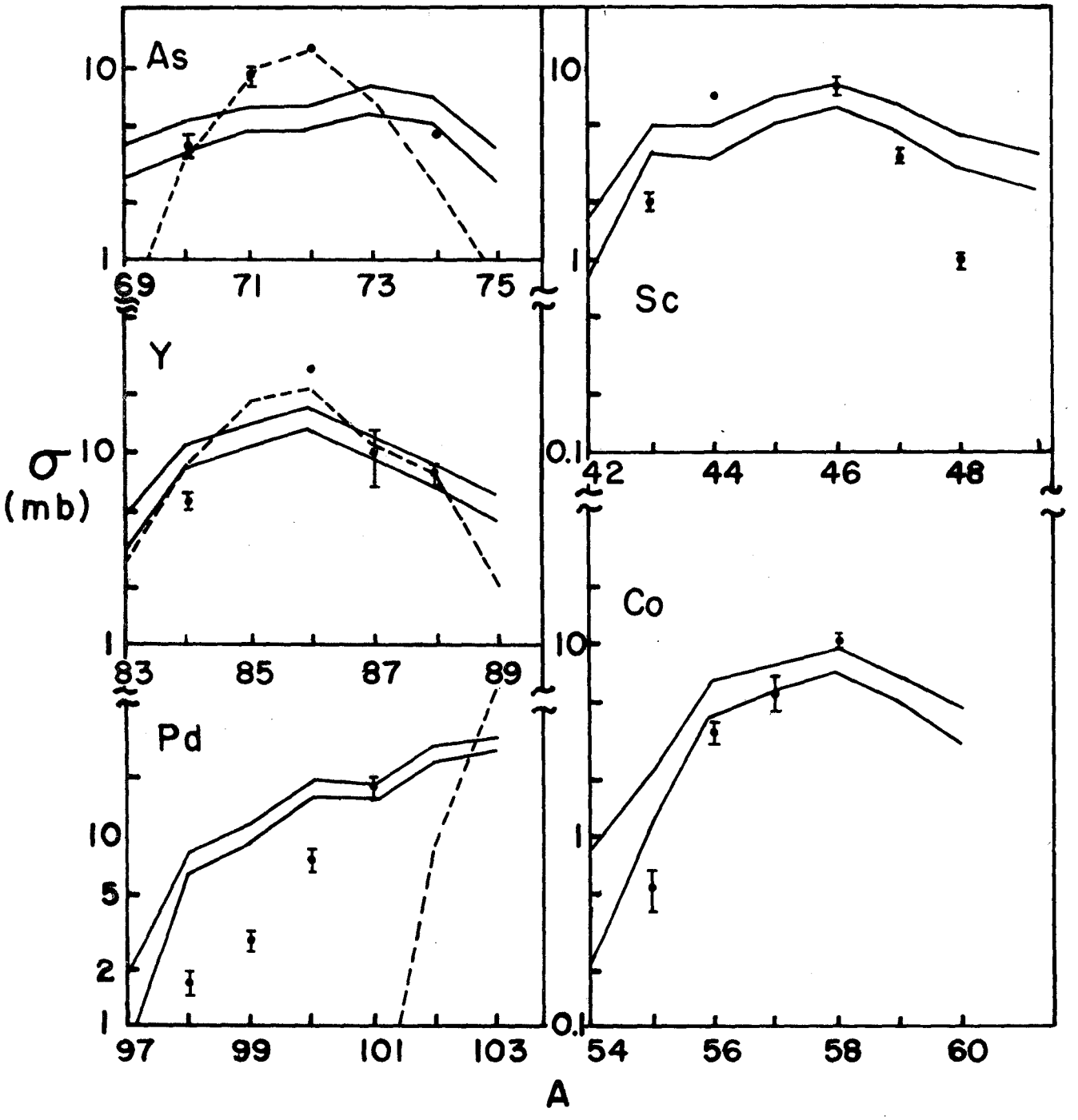


Fig 8
Price et al